Multiple-Quantum Magic-Angle Spinning NMR: A New Method for the Study of Quadrupolar Nuclei in Solids

Ales Medek, John S. Harwood, and Lucio Frydman*

Department of Chemistry (M/C 111), University of Illinois at Chicago, 845 W. Taylor Street, Chicago, Illinois 60607-7061

Received August 24, 1995[⊗]

Abstract: Whereas solid state isotropic spectra can be obtained from spin-$^1/_2$ nuclei by fast magic-angle spinning (MAS), this methodology fails when applied on half-integer quadrupoles due to the presence of non-negligible second-order anisotropic effects. Very recently, however, we have shown that the combined use of MAS and bidimensional multiple-quantum (MQ) spectroscopy can refocus these anisotropies; the present paper discusses theoretical and experimental aspects of this novel MQMAS methodology and illustrates its application on a series of sodium salts. It is shown that even under fixed magnetic field operation, a simple model-free inspection of the peaks in a bidimensional MQMAS NMR spectrum can separate the contributions of isotropic chemical and isotropic quadrupolar shifts for different chemical sites. Moreover the anisotropic line shapes that can be resolved from these spectra are almost unaffected by excitation distortions and can thus be used to discern the values of a site's quadrupolar coupling constant and asymmetry parameter. The conditions that maximize the MQMAS signal-to-noise ratio for a spin-$^3/_2$ are then explored with the aid of a simple analytical model, which can also be used to explain the absence of distortions in the anisotropic line shapes. The MQMAS method thus optimized was applied to the high-resolution ^{23}Na NMR analysis of the multi-site ionic compounds Na_2TeO_3, Na_2SO_3, $Na_3P_5O_{10}$, and Na_2HPO_4; extensions of the MQMAS NMR methodology to the quantitative analysis of inequivalent sites are also discussed and demonstrated.

Introduction

Approximately two out of every three magnetically active nuclides in the Periodic Table possess a half-integer spin number S larger than 1.[1] Interest in the solid phase nuclear magnetic resonance (NMR) spectroscopy of these nuclides is constantly fueled by the roles that several of its members play in a wide variety of important materials such as minerals, ceramics, semiconductors and catalysts.[2−4] By contrast to what happens in the more common case of spin-$^1/_2$ spectroscopy (e.g., ^{1}H, ^{13}C, and ^{31}P NMR), nonspherical quadrupolar nuclei couple not only to the external magnetic field B_0 but also to the surrounding electronic field gradients.[5] Since this anisotropic interaction is usually characterized by coupling constants in the order of several MHz, most NMR transitions of quadrupolar nuclei in the solid phase are too broad to permit the resolution of individual sites. A valuable strategy for improving the resolution of quadrupolar NMR spectra consists of restricting the experiment's excitation to the central $S_z = -^1/_2 \leftrightarrow S_z = +^1/_2$ transition, for which the quadratic form of the quadrupolar Hamiltonian precludes the appearance of first-order effects.[6] Even these transitions, however, can be several tens of kHz wide due to the broadenings introduced via second-order effects, and thus considerable efforts have been invested toward the elimination of these second-order quadrupolar patterns. Initial line narrowing experiments focused on magic-angle spinning (MAS),[7,8] a procedure which although successfully used to cancel out the effects of dipolar and chemical shift anisotropies, fails to remove second-order quadrupole effects.[9,10] Pines, Virlet, and their coworkers explained this limitation in terms of multirank expansions of the relevant Hamiltonians;[11,12] this theoretical approach led to a deeper understanding of the problems involved with the fixed-angle sample spinning of quadrupoles, as well as to practical guidelines for their solution. Indeed the insight provided by this formalism culminated in two new averaging procedures, dynamic-angle spinning (DAS) and double rotation (DOR), which achieved the long-sought goal of high-resolution quadrupolar NMR spectroscopy in solids.[13,14]

Very recently we have demonstrated that a multirank averaging procedure similar to the one occurring in DAS but involving both spatial and spin manipulations of the second-order quadrupole Hamiltonian, can be achieved with the aid of multiple-quantum (MQ) spectroscopy.[15] The resulting approach only requires conventional 2D MAS methods, and since its initial presentation applications of this simple MQMAS methodology have been demonstrated by a growing number of research groups.[16−19] In the present paper we expand on our findings

* To whom correspondence should be addressed.

[⊗] Abstract published in *Advance ACS Abstracts,* December 1, 1995.

(1) Harris, R. K.; Mann, B. E. *NMR and the Periodic Table*; Academic Press: New York, 1970.
(2) Maciel, G. E. *Science* **1984**, *226*, 282.
(3) Oldfield, E.; Kirkpatrick, R. J. *Science* **1985**, *227*, 1537.
(4) Turner, G. L.; Kirkpatrick, R. J.; Risbud, S. H.; Oldfield, E. *Am. Ceram. Soc. Bull.* **1987**, *66*, 656.
(5) Slichter, C. P. *Principles of Nuclear Magnetic Resonance*; Springer-Verlag: New York, 1990.
(6) Abragam, A. *The Principles of Nuclear Magnetism*; Oxford University Press: Oxford, 1985.
(7) Andrew, E. R.; Bradbury, A.; Eades, R. G. *Nature* **1958**, *182*, 1659.
(8) Lowe, I. J. *Phys. Rev. Lett.* **1959**, *2*, 285.
(9) Kundla, E.; Samoson, A.; Lippmaa, E. *Chem. Phys. Lett.* **1981**, *83*, 229.
(10) Ganapathy, S.; Schramm, S.; Oldfield, E. *J. Chem. Phys.* **1982**, *77*, 4360.
(11) Llor, A.; Virlet, J. *Chem. Phys. Lett.* **1988**, *152*, 248.
(12) Wooten, E. W.; Muller, K. T.; Pines, A. *Acc. Chem. Res.* **1992**, *25*, 209.
(13) Chmelka, B. F.; Mueller, K. T.; Pines, A.; Stebbins, J.; Wu, Y.; Zwanziger, J. W. *Nature* **1989**, *339*, 42.
(14) Mueller, K. T.; Sun, B. Q.; Chingas, G. C.; Zwanziger, J. W.; Terao, T.; Pines, A. *J. Magn. Reson.* **1990**, *86*, 470.
(15) Frydman, L.; Harwood, J. S. *J. Am. Chem. Soc.* **1995**, *117*, 5367.
(16) Fernandez, C.; Amoureux, J. P. *Chem. Phys. Lett.* **1995**, *242*, 449.
(17) Fernandez, C.; Amoureux, J. P. *Solid State NMR*, in press.
(18) Youngman, R. E.; Werner-Zwanziger, U.; Zwanziger, J. W. *Z. Naturforscht.*, in press.
(19) Massiot, D.; Tonzo, B.; Trumean, D.; Coutures, J. P.; Virlet, J.; Florian, P.; Grandinetti, P. J.; submitted for publication.

0002-7863/95/1517-12779$09.00/0

concerning the interpretation of MQMAS data and discuss its applications to spin-$^3/_2$ NMR experiments. After briefly reviewing the principles of MQMAS NMR we show how the bidimensional distributions resulting from this experiment can be used to determine, by simple visual inspection, the values of the isotropic quadrupolar and isotropic chemical shifts of inequivalent sites in a powdered sample. Simple line shape simulations can then be performed to retrieve the coupling constants and asymmetry parameters defining the isotropic quadrupolar shifts. The idealized line shapes and high signal-to-noise (S/N) ratios that are observed in MQMAS NMR spectra can be explained using a simple spin-$^3/_2$ analytical model, which is also useful to find the optimized conditions for the experiment's implementation. We conclude by illustrating the analytical power of MQMAS NMR on a series of sodium salts where the different inequivalent sites that are present were identified, their quadrupolar and chemical shift parameters were determined, and their relative abundance quantified.

Experimental Section

All compounds analyzed in the present work were purchased from Alfa AESAR and used without further purification. NMR spectra were acquired at 9.4 T (105 MHz ^{23}Na frequency) on a Bruker AM400 standard-bore spectrometer using the original solution phase hardware, capable of achieving a radiofrequency (rf) nutation rate (ν_1) of 53 kHz. The spectrometer was fitted with a standard-speed 5 mm Doty Sci. probehead; most measurements were done using rotor spinning rates between 5.5 and 7.5 kHz. The ^{81}Br signal of KBr was used to calibrate the magic angle, and the ^{23}Na signal of aqueous NaCl was used as the external frequency reference for all our measurements ($\delta_{NaCl(aq)} = 0$). Unidimensional spectra were collected using short ($\approx 1-2\ \mu s$) excitation pulses. Most 2D data presented in this work involved the acquisition of 128 (t_1) × 256 (t_2) points with dwell times $\Delta t_1 = 30\ \mu s$, $\Delta t_2 = 50\ \mu s$; 240 scans separated by a ca. 1 s relaxation delay and preceded by a number of dummy acquisitions equal to the number of scans in the phase cycle were usually collected for each t_1 increment. Data were processed off the spectrometer in a Power PC computer using the MacRMN program, kindly provided to us by Prof. P. J. Grandinetti (Ohio State University), or using NMRPipe (Molecular Simulations, Inc.) on an SGI computer.

High-Resolution MQMAS NMR Experiment

The possibility of averaging out quadrupole effects via multidimensional multiple-quantum correlations arises when NMR experiments can be described by an energy diagram of the type shown in Figure 1, involving a dominant Zeeman interaction

$$\mathcal{H}_z = -\nu_L S_z \tag{1}$$

perturbed by a smaller quadrupolar Hamiltonian

$$\mathcal{H}_Q = \nu_Q(\theta,\varphi)[3S_z^2 - S(S+1)] \tag{2}$$

An MQMAS NMR experiment therefore requires a high-field scenario where the Larmor frequency ν_L is large compared to the quadrupolar frequencies

$$\nu_Q(\theta,\varphi) = \frac{e^2qQ/h}{2S(2S-1)}\frac{(3\cos^2\theta - 1 + \eta\sin^2\theta\cos 2\varphi)}{2} \tag{3}$$

described in terms of a nuclear site quadrupole coupling constant (e^2qQ/h), an asymmetry parameter (η), and angles (θ,φ) defining the orientation of the external field B_o within the principal axis system of the quadrupolar tensor. This situation is often

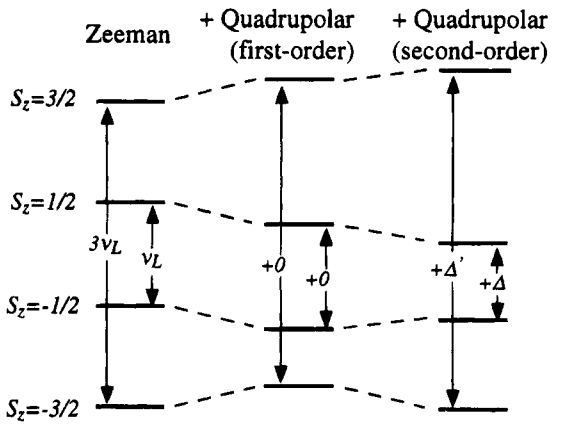

Figure 1. Energy level diagram of a spin-$^3/_2$, showing the cumulative effects of the first- and second-order quadrupole effects on a dominant Zeeman interaction. The arrows indicate transitions between $S_z = +m$ and $S_z = -m$ states, which are unaffected to first order by the quadrupolar Hamiltonian.

encountered in the spectroscopy of a variety of nuclei such as ^{23}Na, ^{11}B, ^{27}Al, and ^{17}O. The proportionality of $\mathcal{H}_Q$ to S_z^2 will in these cases cancel the presence of first-order quadrupolar effects on any $S_z = -m \leftrightarrow S_z = +m$ energy transition; these transition frequencies, however, will still be broadened by second-order effects Δ that are proportional to $||\mathcal{H}_Q^2||/||\mathcal{H}_z||$. A common approach employed to reduce these second-order effects consists of rapidly spinning the sample about an axis β degrees away from B_o. Then, if one allows for the existence of an isotropic chemical shift (ν^{CS}) and disregards the effects of time-dependent oscillatory terms, the evolution undergone by a $-m \leftrightarrow +m$ spin coherence after excitation can be described by a multirank expansion of its phase ϕ:[15,20,21]

$$\phi(m,\beta,t) = \nu^{CS}\,2mt + \nu_0^Q C_0^S(m)t + \nu_2^Q(\theta,\varphi)C_2^S(m)P_2(\cos\beta)t + \nu_4^Q(\theta,\varphi)C_4^S(m)P_4(\cos\beta)t \tag{4}$$

where

$$C_0^S(m) = 2m[S(S+1) - 3m^2] \tag{5a}$$

$$C_2^S(m) = 2m[8S(S+1) - 12m^2 - 3] \tag{5b}$$

$$C_4^S(m) = 2m[18S(S+1) - 34m^2 - 5] \tag{5c}$$

are zero-, second- and fourth-rank coefficients depending on the spin S and order m of the transition,

$$P_2(\cos\beta) = (3\cos^2\beta - 1)/2 \tag{6a}$$

$$P_4(\cos\beta) = (35\cos^4\beta - 30\cos^2\beta + 3)/8 \tag{6b}$$

are second- and fourth-order Legèndre polynomials of cosβ,

$$\nu_0^Q = -\frac{(e^2qQ/h)^2(3+\eta^2)}{10\nu_L[2S(2S-1)]^2} \tag{7}$$

is the isotropic (or zero-rank) quadrupolar shift, and $\nu_2^Q(\theta,\varphi)$, $\nu_4^Q(\theta,\varphi)$ are second- and fourth-rank angular-dependent frequencies responsible for the observed line broadening.

(20) Lefebvre, F.; Amoreux, J. P.; Fernandez, C.; Deronane, E. G. *J. Chem. Phys.* **1987**, *86*, 6070.
(21) Sun, B. Q. Ph.D. Thesis, Materials Science Division, Lawrence Berkeley Laboratory, University of California, 1991.

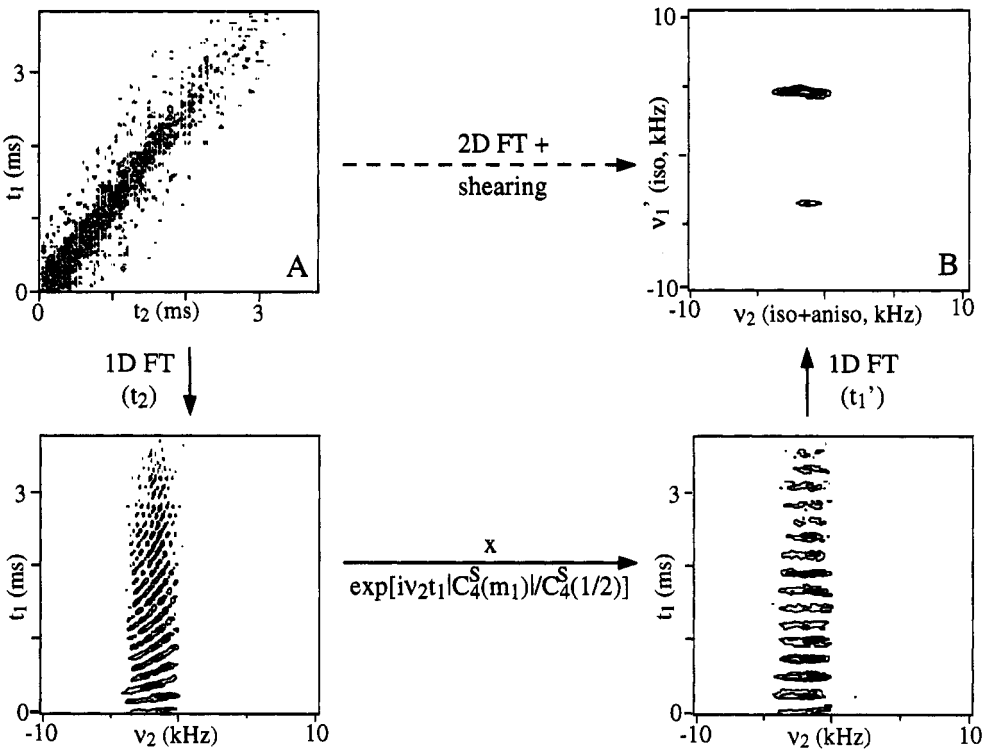

Figure 2. Two-dimensional ^{23}Na MQMAS NMR of $Na_2C_2O_4$. (A) Triple-/single-quantum correlation experiment obtained using the two-pulse sequence shown in Scheme 1. (B) Isotropic/anisotropic correlation spectrum obtained by Fourier transformation and shearing of the time-domain data; the peak at $\nu'_1 \approx 4$ kHz corresponds to the main resonance, the peak at $\nu'_1 = -3$ kHz is a spinning sideband. The shearing was implemented as illustrated in the bottom part of the figure, via a first-order t_1-dependent phase correction along ν_2.

Since no spinning axis β can simultaneously cancel out $P_2(\cos\beta)$ and $P_4(\cos\beta)$, a residual anisotropic broadening always characterizes fixed-angle quadrupolar NMR experiments. This resolution limitation is resolved in DAS by allowing spins to evolve during consecutive times t_1 and t_2 at spinning angles β_1 and β_2,[14] chosen so as to simultaneously fulfill the second- and fourth-rank averaging condition

$$[P_2(\cos\beta_1)t_1,P_4(\cos\beta_1)t_1] + [P_2(\cos\beta_2)t_2,P_4(\cos\beta_2)t_2] = [0,0] \quad (8)$$

For a given $-m \leftrightarrow +m$ transition there are a number of $\{\beta_1,\beta_2\}$ angles that can meet this condition,[21] thereby leading at times $t_1 + t_2$ to signals that are free from all anisotropic contributions. In a completely analogous manner it is possible to propose an experiment whereby for a fixed spinning angle β, spins are allowed to evolve during initial and final times under the effects of two transitions m_1 and m_2, chosen so as to fulfill the second-order averaging

$$[C_2^S(m_1)t_1,C_4^S(m_1)t_1] + [C_2^S(m_2)t_2,C_4^S(m_2)t_2] = [0,0] \quad (9)$$

This condition can be met for a variety of spinning angles among which the most convenient one is $\beta = 54.7°$ (the MAS case), as then the hitherto neglected anisotropic shift and dipolar interactions are also effectively averaged away by spinning. The resulting MQMAS approach can then result in very sharp half-integer quadrupole resonances, whose line broadening is restricted to relaxation or residual higher order effects.

Even though selection rules considerations restrict the practical implementation of eq 9 to the $m_2 = -1/2 \leftrightarrow m_2 = +1/2$ case, cycling of the irradiation and demodulation rf phases can still allow one to choose the apparent sense of multiple-quantum precession during t_1. The evolution phases ϕ_1 and ϕ_2 correlated in 2D MQMAS can therefore be written as

$$\phi_1 = \nu_1 t_1 = \pm[2m_1\nu^{CS} + C_0^S(m_1)\nu_0^Q + C_4^S(m_1)P_4(\cos\beta_m)\nu_4^Q(\theta,\varphi)]t_1 \quad (10a)$$

$$\phi_2 = \nu_2 t_2 = [\nu^{CS} + C_0^S(1/2)\nu_0^Q + C_4^S(1/2)P_4(\cos\beta_m)\nu_4^Q(\theta,\varphi)]t_2 \quad (10b)$$

Since $C_4^S(1/2)$ is always a positive number the value of $C_4^S(m_1)$ will dictate the sign of ϕ_1 that needs to be chosen in order to achieve the refocusing of the anisotropic terms: when $C_4^S(m_1)$ is negative the plus sign will generate a refocusing, while when this coefficient is positive the minus sign will be effective. In both cases a purely isotropic echo formation can be expected at

$$t_2 = |C_4^S(m_1)|C_4^S(1/2)|t_1 \quad (11)$$

These predictions are fully confirmed by experimental observations. Figure 2A for instance illustrates for a ^{23}Na NMR experiment on sodium oxalate ($S = m_1 = 3/2$ case), the refocusing of the fast-decaying anisotropic evolution that takes place along the ideal $t_2 = (42/54)t_1$ line. Conventional 2D Fourier processing of these data leads to a correlation plot between ν_1 and ν_2; although these two frequencies possess an anisotropic component (eq 10), their anisotropies are proportional to each other and thus place inequivalent sites along sharp, parallel spectral ridges. A practical alternative to this mode of displaying MQMAS data is to carry out a shearing transformation capable of transforming the (ν_1,ν_2)-domain spectrum into a distribution like the one shown in Figure 2B, possessing a purely isotropic frequency component along one of the spectral axes. Of the different ways in which such a transformation can be carried out the most convenient one is by employing a linear phase correction in the mixed (t_1,ν_2)-domain, as this approach requires no interpolations while avoiding S/N losses associated

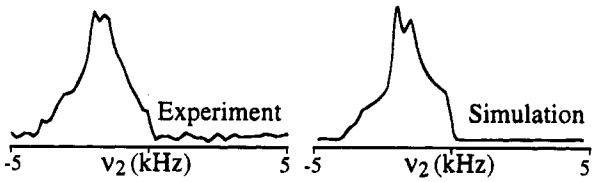

Figure 3. Comparison between the experimental powder pattern extracted from Figure 2B for the $Na_2C_2O_4$ centerband and the idealized line shape simulation (eq 12b) predicted by the literature quadrupolar parameters.

with delayed acquisitions.[22] The resulting processing protocol leads to a 2D spectral distribution where the ν_2 frequency of eq 10b is now correlated with a purely isotropic frequency $\nu'_1 = \nu_1 + \nu_2|C_4^S(m_1)|/C_4^S(^1/_2)$; for the specific case of a triple-/single-quantum correlation experiment on a spin-$^3/_2$ the two correlated frequencies are then given by

$$\nu'_1 = \frac{34\nu^{CS} - 60\nu_0^Q}{9} \qquad (12a)$$

$$\nu_2 = \nu^{CS} + 3\nu_0^Q - 21\nu_4^Q(\theta,\varphi) \qquad (12b)$$

Inspection of the functional form of $\nu_4^Q(\theta,\varphi)$ shows that in a random powder distribution, its center of mass is identically zero; a model-free first moment analysis of a site's centerband along the ν'_1- and ν_2-domains can therefore provide a straightforward way of discriminating the isotropic chemical from the isotropic quadrupolar shifts contributions. In the case of $Na_2C_2O_4$ (Figure 2B) the average frequencies that can be measured are $\langle\nu'_1\rangle = 4240$ Hz, $\langle\nu_2\rangle = -1630$ Hz, from which eqs 12 lead to $\nu_0^Q = -577$ Hz and $\delta^{CS} = 10^6 \times \nu^{CS}/\nu_L = 1.0$. It is worth noting that previous single-quantum approaches required variable magnetic field measurements or iterative computational line shape fits for achieving a similar distinction among the isotropic quadrupolar and shielding contributions. Furthermore, the specific contributions that the quadrupolar coupling constant e^2qQ/h and the asymmetry parameter η make to the value of ν_0^Q can be discerned by fitting anisotropic line shapes extracted along the ν_2 domain. Figure 3 illustrates such fitting procedure for $Na_2C_2O_4$ using the literature values $e^2qQ/h = (2.6 \pm 0.1)$ MHz, $\eta = (0.7 \pm 0.1)$.[21] Notably, idealized simulations of this kind match remarkably well the experimental line shapes in spite of potential imperfections in the mechanism of the multiple-quantum excitation. This fact lends support to the reliability of the MQMAS NMR approach, while raising important questions about the spin dynamics involved in the MQMAS experiment.

MQMAS NMR: Pulse Sequence Considerations

It follows from the arguments discussed in the preceding paragraph that a triple-/single-quantum 2D MAS correlation experiment can always yield a high-resolution quadrupolar NMR spectrum, provided that the apparent sense of evolution is kept constant during t_1 and t_2 for $S = ^3/_2$, and is reversed for the remaining ($S = ^5/_2, ^7/_2, \ldots$) cases. In coherence transfer terminology this means that for any spin number the acquisition of signals arising from the $0 \rightarrow \pm3$ (t_1) $\rightarrow -1$ (t_2) pathways will always afford a high-resolution spectrum; discrimination between the echo and anti-echo signals of these pathways can then be carried out via off-resonance irradiation, by TPPI, or using the method of States et al.[17,19,22] There are in principle

(22) Ernst, R. R.; Bodenhausen, G.; Wokaun, A. *Principles of Nuclear Magnetic Resonance in One and Two Dimensions*; Clarendon: Oxford, 1987.

Scheme 1

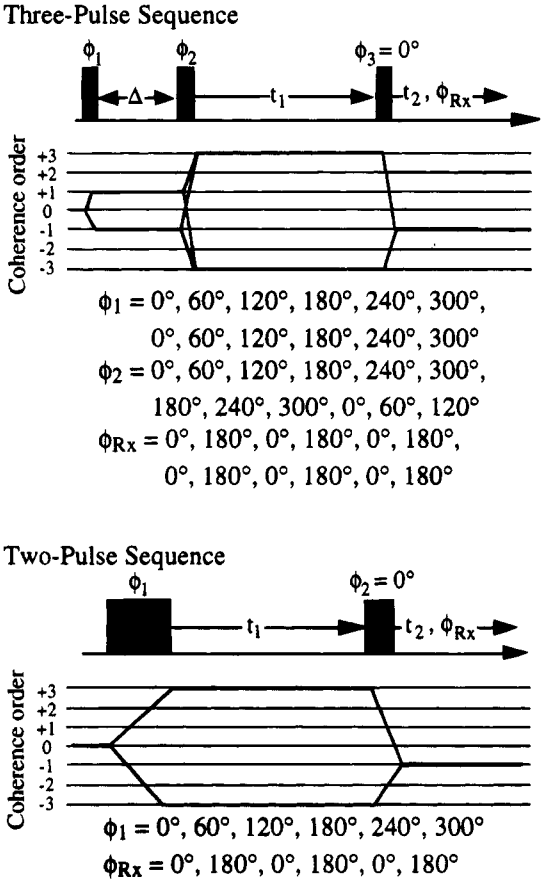

Table 1. MQMAS NMR S/N Ratios Measured for Selected Sodium Resonances under Similar Conditions Using Three-/Two-Pulse Sequences

compound	three-pulse sequence	two-pulse sequence
$Na_2C_2O_4$	31	37
Na_2TeO_3 (site 1)	70	150
$Na_5P_3O_{10}$ (site 1)	63	200
Na_2HPO_4 (site 1)	66	85

two pulse sequences that can be used to obtain this type of 2D MQMAS quadrupolar correlations: the three-pulse sequence normally used within the context of liquid-phase experiments such as DQF-COSY and INADEQUATE,[22,23] and the two-pulse approach initially exemplified by Vega and Pines for double-quantum ^2H NMR[24] and subsequently extended by different researchers to the study of half integer quadrupoles.[25-28] The timing and basic phase cycles demanded by these pulse sequences for implementing the $0 \rightarrow \pm3$ (t_1) $\rightarrow -1$ (t_2) MQMAS selection, are summarized in Scheme 1. Both pulse sequences have already been successfully applied to retrieve high resolution MQMAS NMR spectra from $S = ^3/_2$ and $S = ^5/_2$ quadrupoles;[15-19] we have tested their ^{23}Na MQMAS NMR performance under comparable conditions of optimization on a series of sodium compounds, and observed the relative S/N ratios summarized in Table 1. These data suggest that, at least in spin systems like ^{23}Na where quadrupolar effects dominate the MAS spectrum, the two-pulse approach can in general yield

(23) Bodenhausen, G. *Prog. Nucl. Magn. Reson. Spectrosc.* **1981**, *14*, 137.
(24) Vega, S.; Pines, A. *J. Chem. Phys.* **1977**, *66*, 5624.
(25) Wokaun, A.; Ernst, R. R. *J. Chem. Phys.* **1977**, *67*, 1752.
(26) Vega, S. *J. Chem. Phys.* **1978**, *68*, 5518.
(27) Vega, S.; Naor, Y. J. *J. Chem. Phys.* **1981**, *75*, 75.
(28) Nielsen, N. C.; Bildsøe, H.; Jakobsen, H. J. *Chem. Phys. Lett.* **1992**, *191*, 205.

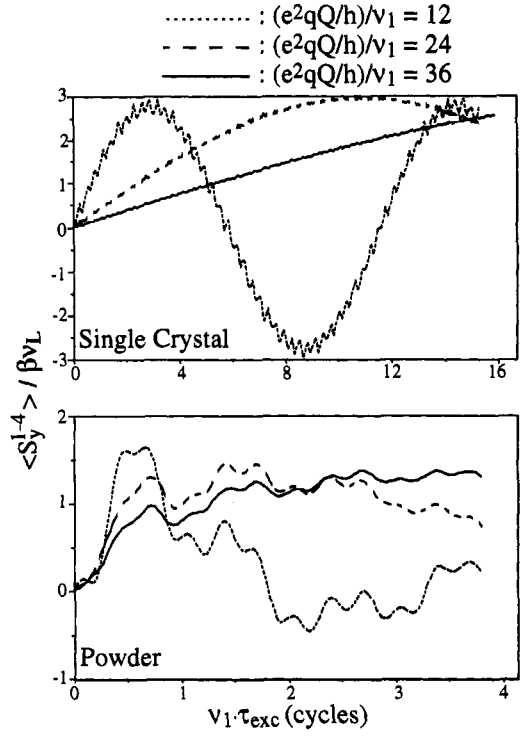

Figure 4. Triple-quantum nutation behavior calculated for a spin-$^3/_2$ in a single-crystal ($\theta = \varphi = 0$, top) and in a powdered sample (bottom) for different $(e^2qQ/h)/\nu_1$ values. For all calculations quadrupolar parameters $e^2qQ/h = 2.4$ MHz and $\eta = 0$ were used; the values assumed for the rf nutation field were 200 kHz (dotted lines), 100 kHz (dashed lines), and 67 kHz (continuous lines).

spectra possessing higher S/N ratios than its three-pulse counterpart. This in turn opens up practical questions regarding the optimization of this pulse sequence, as well as regarding the artifacts that it may originate when applied on polycrystalline samples possessing a distribution of coupling constants.

The general answers to these questions for arbitrary spin numbers, coupling parameters, spinning rates, and rf powers require the propagation of large density matrices evolving under the effects of noncommuting time-dependent Hamiltonians; this full computational treatment will be presented in an upcoming publication.[29] General insight about the behavior of the two-pulse sequence can still be obtained from an analytical theoretical treatment similar to the one employed in the past for the case of single-crystals[27] and which we extend here to understand the mechanism of MQMAS experiments on powders. Specifically, we investigate the way in which an on-resonance irradiation Hamiltonian given in the usual rotating frame by

$$\mathcal{H}_{irr} = \nu_Q(\theta,\varphi)(3S_z^2 - {}^{15}/_4) + \nu_1 S_x \qquad (13)$$

can elicit MQMAS NMR spectra from spin-$^3/_2$. The first stage of the experiment involves the excitation of an ensemble from its equilibrium state $\rho_{eq} = \beta\nu_L S_z$ into triple-quantum coherences. If one disregards the effects of spinning, this excitation process can be quantified by calculating the time evolution of the density matrix

$$\rho(\tau_{exc}) = e^{-i\mathcal{H}_{irr}\tau_{exc}}\rho_{eq}e^{i\mathcal{H}_{irr}\tau_{exc}} \qquad (14)$$

where τ_{exc} is the length of the excitation pulse. The diagonalization involved in this density matrix propagation can be carried out in a closed form by transforming $\mathcal{H}_{irr}$ into the eigenbase of the S_x operator[27,30] and leads to a solution of eq 14 given by a complex superposition of time-dependent coherences and populations. Out of all these different terms our attention is centered

(29) Fernandez, C.; Amoureux, J. P.; Frydman, L.; manuscript in preparation.

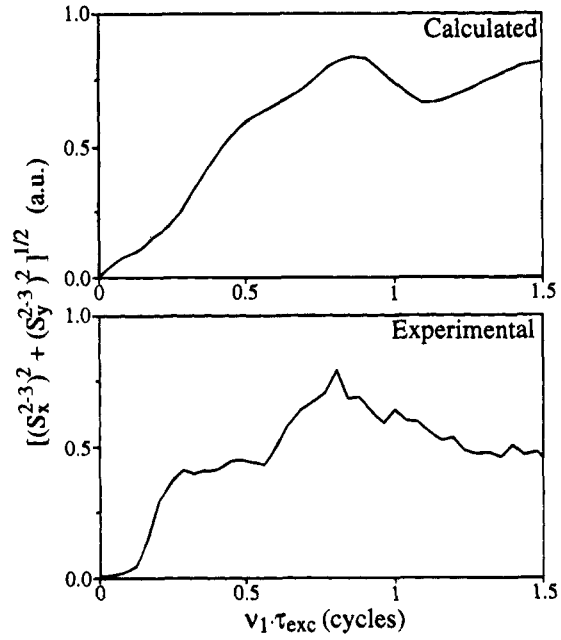

Figure 5. Comparison between the excitation-pulse dependence predicted for a powder by eq 15 and the experimental ^{23}Na MQMAS NMR behavior observed for $Na_2C_2O_4$. The calculations assumed $e^2qQ/h = 2.4$ MHz, $\eta = 0$, $\nu_1 = 50$ kHz; experimental data were acquired using a two-pulse MQMAS sequence (Scheme 1) with an evolution time $t_1 = 400$ μs and a second pulse-length (τ_{conv}) of 4 μs. All data are plotted as the magnitude value of the multiple-quantum echo intensity.

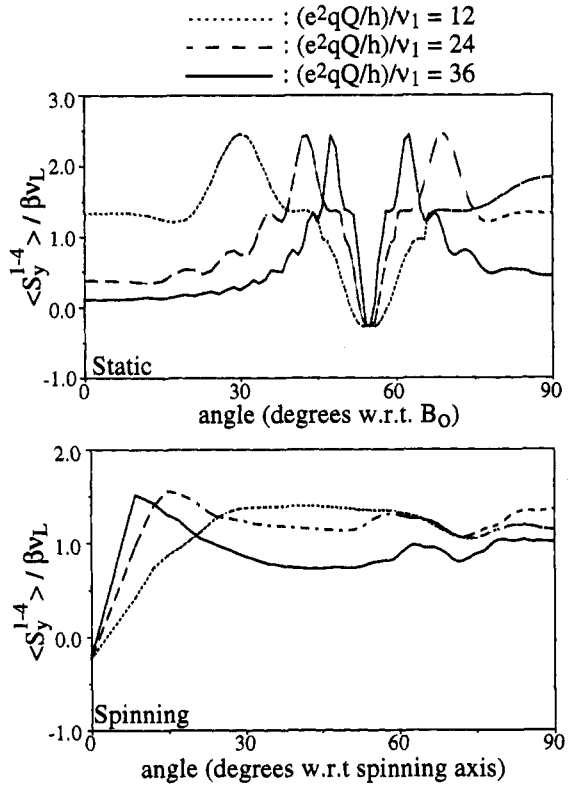

Figure 6. Angular dependence of triple-quantum excitation profiles in static and spinning samples, calculated for different $(e^2qQ/h)/\nu_1$ ratios. The computations assumed an excitation pulse $\nu_1\tau_{exc} = 0.8$ cycles and quadrupolar parameters $e^2qQ/h = 2.4$ MHz, $\eta = 0$.

(30) Jannsen, R.; Veeman, W. S. *J. Chem. Soc., Faraday Trans.* **1988**, *84*, 3747.

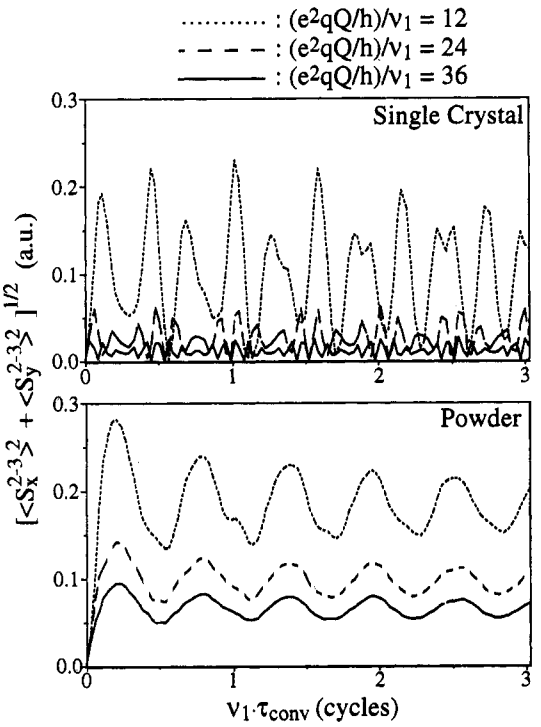

Figure 7. Dependence of the triple- to single-quantum conversion process for a spin-$^3/_2$ ensemble on single-crystal (top) and powdered (bottom) samples, calculated for different $(e^2qQ/h)/\nu_1$ ratios. Computations assumed an initial condition $S_x^{1-4} = S_y^{1-4} = 1$ and quadrupolar parameters $e^2qQ/h = 2.4$ MHz, $\eta = 0$.

on elements connecting the $S_z = -^3/_2$ and $S_z = +^3/_2$ states, which are conveniently described by the fictitious spin-$^1/_2$ operator set $\{S_i^{1-4}\}_{i=x,y,z}$ that defines the triple-quantum subspace. The relevant time evolution can then be concisely described as

$$\beta\nu_L S_z \xrightarrow{\mathscr{H}_{irr}\tau_{exc}} 0S_x^{1-4} + \beta\nu_L[C_1 \sin(\lambda_1 - \lambda_3)\tau_{exc} + C_2 \sin(\lambda_1 - \lambda_4)\tau_{exc} + C_3 \sin(\lambda_2 - \lambda_3)\tau_{exc} + C_4 \sin(\lambda_2 - \lambda_4)\tau_{exc}]S_y^{1-4} \quad (15)$$

where $\{\lambda_i\}_{i=1,4}$ are the eigenvalues of $\mathscr{H}_{irr}$ and $\{C_i\}_{i=1,4}$ are coefficients depending on its eigenvectors. As the ratio between the rate of nutation ν_1 and the quadrupolar coupling e^2qQ/h decreases, C_1 tends toward a value of 3.0 while all other coefficients tend to zero; this leaves $\lambda_1 - \lambda_3$ as the dominant nutation frequency of the excitation, which for a single-crystal will then proceed like a normal spin-$^1/_2$ rf nutation whose precession frequency has been scaled by a factor proportional to $[\nu_1/(e^2qQ/h)]^2$ and whose amplitude reaches $3\beta\nu_L$ instead of the usual $\beta\nu_L$ value (Figure 4, top). Of relevance to the MQMAS experiment is the evolution of spins in a powdered sample containing a distribution of coupling constants, which can be calculated from this formalism using a weighted superposition of single-crystallite curves. Notably, although the resulting powder curves lack the long-term sinusoidal behavior of their single-crystal counterparts, they still display at short excitation times the buildup of substantial triple-quantum coherences that can even exceed the signal available from an ideal central-transition excitation (Figure 4, bottom). Moreover, a local maximum of excitation can be achieved over a range of $(e^2qQ/h)/\nu_1$ values for $\nu_1\tau_{exc} \approx 0.8$ cycles, thus indicating the suitability of using this type of excitation pulse for maximizing S/N ratios in the study of unknown samples. For the nutation rates normally used in solid phase NMR these pulse lengths fall in the 5−10 μs range, times that are much shorter than

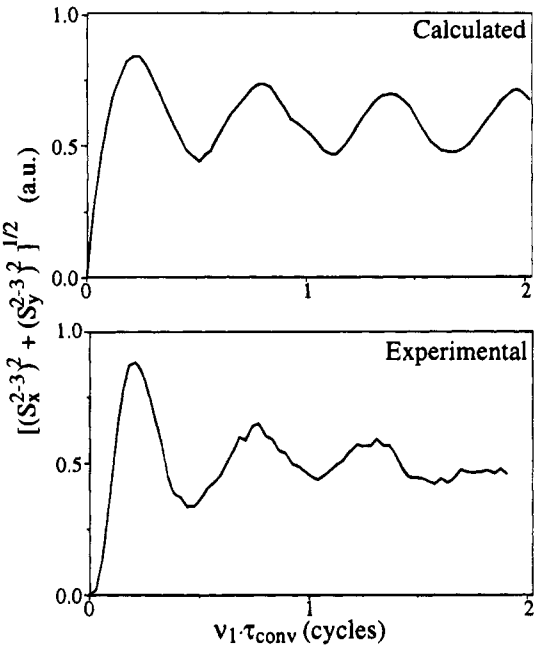

Figure 8. Comparison between the conversion-pulse dependence predicted by eqs 16 for a spin-$^3/_2$ powder, and experimental MQMAS NMR results observed for $Na_2C_2O_4$. Calculations were based on the same parameters as in Figure 5; experimental data were acquired using an excitation pulse $\tau_{exc} = 9$ μs, a fixed evolution time $t_1 = 400$ μs, and are presented as the magnitude of the multiple-quantum echo intensity.

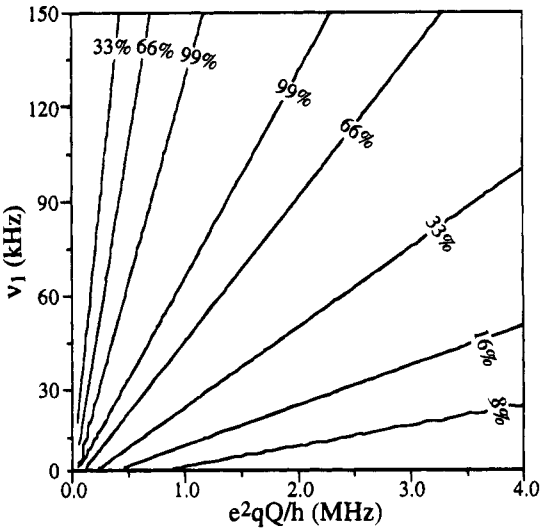

Figure 9. Scaling behavior of the total MQMAS signal predicted by eqs 15 and 16 as a function of the strength of quadrupole coupling constants and the rates of rf nutation. Calculations involved a powder averaging of 500 orientations and assumed $\eta = 0$, $\nu_1\tau_{exc} = 0.8$ cycles, $\nu_1\tau_{conv} = 0.2$ cycles and $t_1 = 0$; contours are given as percentages with respect to the maximum calculated intensity.

typical rotor periods (150−300 μs) and which therefore justify our use of a static-Hamiltonian approach. The predictions of this simple theory are indeed in good agreement with experimental MQMAS observations (Figure 5).

Another important aspect of the 2D MQMAS experiment that this simple theoretical approach can help to explain concerns the negligible distortions that are observed in the final anisotropic spectral line shapes (e.g., Figure 3). Equation 15 predicts that the multiple-quantum excitation of a static powder will be highly anisotropic, with faster rates of nutation for crystallites whose quadrupole tensors are oriented in the neighborhood of the magic angle ($\nu_Q \approx 0$) and slower rates for the remaining

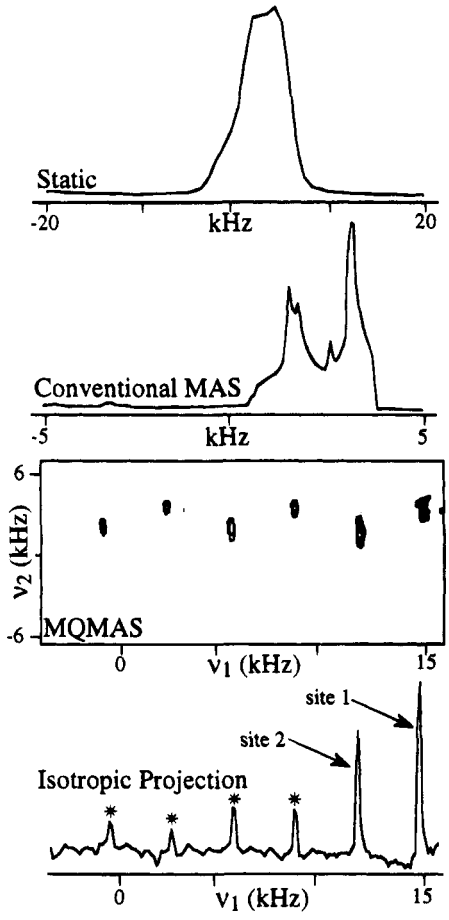

Figure 10. ^{23}Na NMR spectra of polycrystalline Na_2TeO_3 acquired under different conditions. The bottom trace corresponds to the projection of the sheared 2D MQMAS spectrum onto the isotropic (ν_1) axis; asterisks correspond to spinning sidebands.

orientations (Figure 6, top). In a sample that spins at rates exceeding the magnitude of second-order quadrupole effects, however, it is the orientation of these tensors with respect to the axis of macroscopic rotation what will determine the resonance frequency of the spins. A simple transformation allows one to include this consideration into the time-independent triple-quantum excitation formalism described by eq 15; when this is done a marked improvement in the homogeneity of the powder excitation can be observed (Figure 6, bottom), thus explaining the ideality of line shapes obtained in the MQMAS NMR observations.

The same theoretical framework employed in these excitation analyses can be used to understand the conversion of triple-quantum coherences into the single-quantum central transition observables S_x^{2-3}, S_y^{2-3} by effects of the second pulse. There are now two different possible initial states, S_x^{1-4} and S_y^{1-4}, which transform under the effects of an rf irradiation lasting for a period τ_{conv} as

$$S_x^{1-4} \xrightarrow{\mathcal{H}_{irr}\tau_{conv}} \{C_5[1 - \cos(\lambda_1 - \lambda_2)\tau_{conv}] + C_6[1 - \cos(\lambda_3 - \lambda_4)\tau_{conv}]\}S_x^{2-3} + 0S_y^{2-3} \quad (16a)$$

$$S_y^{1-4} \xrightarrow{\mathcal{H}_{irr}\tau_{conv}} 0S_x^{2-3} + C_7[\cos(\lambda_1 - \lambda_3)\tau_{conv} + \cos(\lambda_2 - \lambda_4)\tau_{conv} - \cos(\lambda_1 - \lambda_4)\tau_{conv} - \cos(\lambda_2 - \lambda_3)\tau_{conv}]S_y^{2-3} \quad (16b)$$

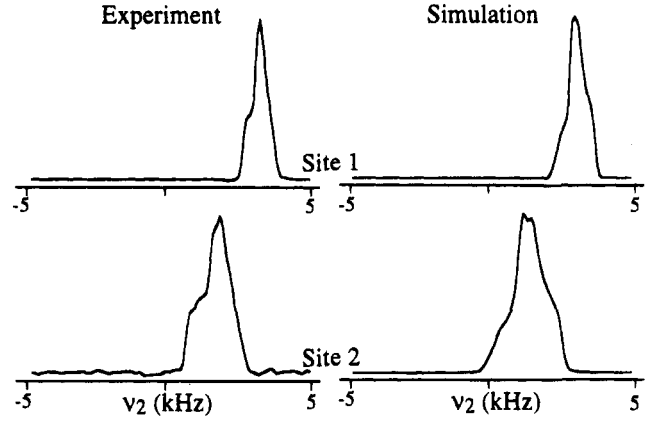

Figure 11. Comparison between the experimental anisotropic line shapes observed for each of the two sites of Na_2TeO_3, and best fit simulated distributions obtained using eq 12b.

By contrast to what happened in the case of the excitation, all $\{C_i\}_{i=5,7}$ coefficients involved in this conversion process tend rapidly toward zero as the $(e^2qQ/h)/\nu_1$ ratio increases. This fact combined with the absence of a dominant oscillating term will make the triple- to single-quantum conversion process inefficient even in the case of single-crystals (Figure 7, top), a behavior that is strongly reminiscent of the related case of satellite transition excitations by on-resonance irradiation. When considering the effects of the pulse on powdered samples, it is possible to detect again a coherent short-time superposition of the single-crystal curves, which leads to substantial amounts of triple- to single-quantum conversion for pulse lengths fulfilling $\nu_1\tau_{conv} \approx 0.2$ cycles (Figure 7, bottom). This approximate time-independent model is again well supported by ^{23}Na MQMAS NMR results (Figure 8), owing to the difference between the time-scale of the rf pulses involved in the conversion process and the duration of a rotor period.

It is worth concluding these pulse sequence considerations by indicating the importance of using the highest available nutation fields for improving the S/N ratio of an MQMAS experiment, mainly as a consequence of the relative inefficiency of the last-pulse conversion process. For instance for the optimized excitation conditions calculated above ($\nu_1\tau_{exc} \approx 0.8$ cycles, $\nu_1\tau_{conv} \approx 0.2$ cycles), Figure 9 illustrates the benefit that can be achieved by increasing the rates of rf nutation; note that for the range of e^2qQ/h values normally encountered in ^{23}Na NMR (1.0 to 4.0 MHz), increasing the strength of the rf field from 30 to 100 kHz can result in a ca. ten-fold reduction in the duration of an MQMAS acquisition. The signal strength that under these high-power irradiations can then be observed in the initial time-domain acquisition of a 2D MQMAS measurement reaches up to 20% of the amplitude characterizing the corresponding single-pulse MAS signal. Only in the case of very small coupling constants may the use of very strong rf fields be detrimental to the overall S/N ratio of a spectrum; in these cases, however, second-order effects can be expected to be fairly small and susceptible to averaging by conventional MAS.

Results

Having discussed the principles of MQMAS NMR, the shielding and quadrupole information that the experiment can provide, and optimized conditions for the experiment's implementation on spin-$^3/_2$ nuclei, we illustrate now the usefulness of the method with a series of results obtained on multisite inorganic sodium salts. The typical resolution enhancement that can be expected from MQMAS can be appreciated in Figure

Table 2. Site-Resolved NMR Parameters Determined by MQMAS for Different Sodium Salts[a]

compound	site	δ^{CS} (ppm) (lit. value)[b]	ν_0^Q (Hz)	e^2qQ/h (MHz) (lit. value)[b]	η (lit. value)[b]
Na_2TeO_3	Na(1)	24.5 ± 1 (17.0)[c]	−220 ± 5	1.5 ± 0.1 (1.4)	0.8 ± 0.2 (0.9)
	Na(2)	14.0 ± 1 (5.8)[c]	−350 ± 5	1.9 ± 0.1 (1.8)	0.8 ± 0.2 (0.8)
Na_2SO_3	Na(1)	0.5 ± 1 (−7.5)[c]	−100 ± 5	1.1 ± 0.1 (1.2)	0.3 ± 0.2 (0)
	Na(2)	5.5 ± 1 (−1.4)[c]	>−5, <0	<0.1 (0.2)	− (0)
	Na(3)	5.5 ± 1 (−0.8)[c]	−125 ± 5	1.25 ± 0.1	0.3 ± 0.2 (0)
$Na_5P_3O_{10}$	Na(1)	−14.5 ± 1	−290 ± 5	1.75 ± 0.1	0.8 ± 0.2
	Na(2)	−4.5 ± 2	−200 ± 10	1.4 ± 0.2	0.9 ± 0.2
Na_2HPO_4	Na(1)	6.0 ± 2 (6.2)	−160 ± 5	1.4 ± 0.1 (1.4)	0.2 ± 0.2 (0.2)
	Na(2)	5.5 ± 1 (5.5)	−370 ± 10	2.0 ± 0.2 (2.1)	0.7 ± 0.2 (0.7)
	Na(3)	7.5 ± 1 (7.2)	−1100 ± 25	3.7 ± 0.3 (3.7)	0.3 ± 0.2 (0.3)

[a] Errors are reported on the basis of the accuracy estimated for experimental observations. [b] Figures in parentheses correspond to values reported in the literature. [c] These literature values were reported using solid ^{23}NaCl as reference: $\delta_{NaCl(solid)} = 0$.

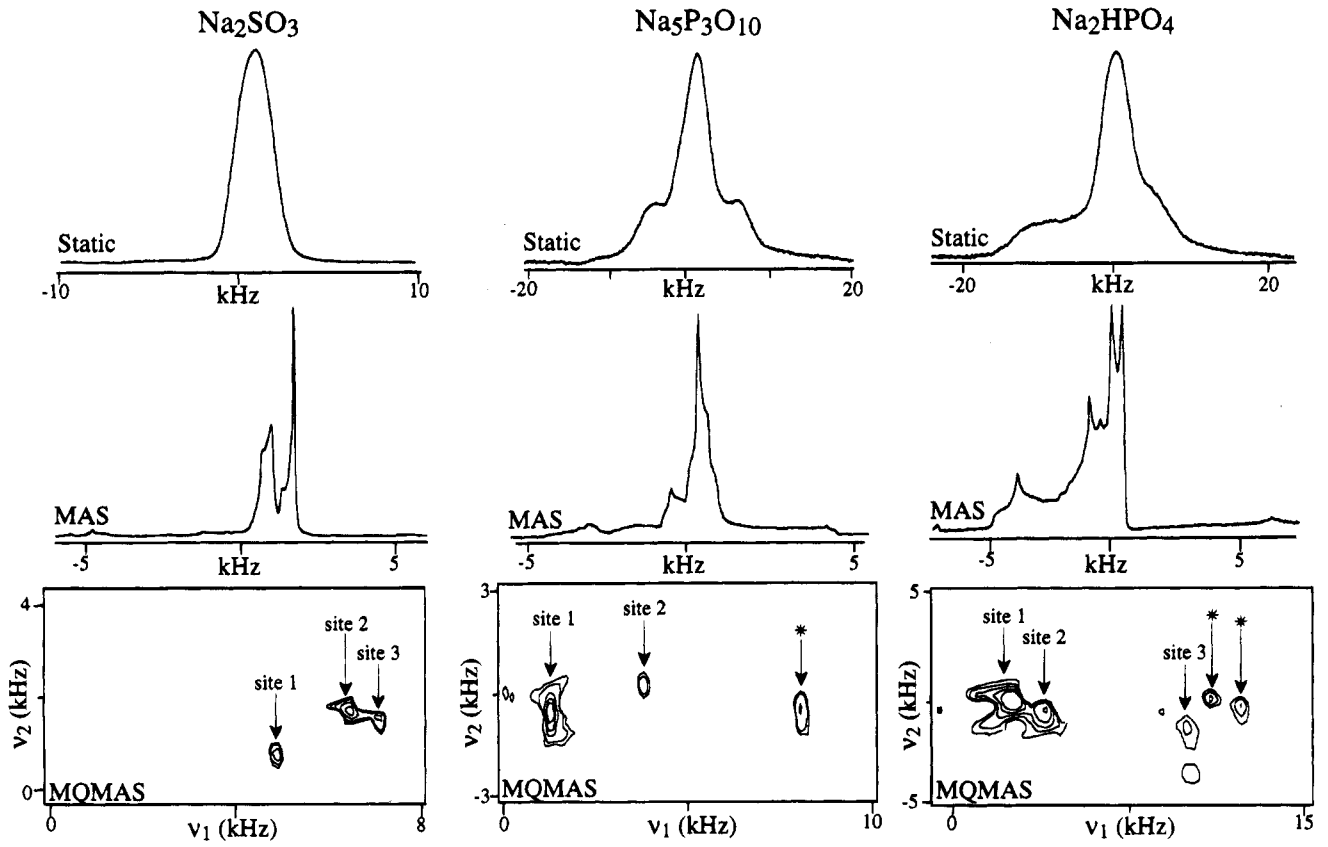

Figure 12. Comparison between the static, MAS, and MQMAS ^{23}Na NMR spectra of multisite sodium salts. Contour levels in the bidimensional plots were taken at 70, 35, 16, 8, and 4% of the maximum spectral intensities; asterisks indicate the spinning sidebands.

10, which compares the line shapes that are observed when a Na_2TeO_3 sample is analyzed by static, by conventional MAS and by 2D MQMAS NMR methods. The static peak is approximately 10 kHz wide and its line shape is dominated by a combination of quadrupolar and homonuclear dipolar broadenings. The latter are removed almost completely by MAS, revealing a series of second-order powder patterns with well-defined singularities. Although the number of sites giving origin to this MAS line shape is not immediately apparent from the spectrum, the two sites existing in Na_2TeO_3 can be clearly distinguished in the sheared representation of the 2D MQMAS NMR spectrum. Also noticeable are strong families of spinning sidebands associated to each isotropic resonance, arising most likely as a consequence of time modulations introduced on the magnified multiple-quantum anisotropic chemical shifts. All resonances along the isotropic dimension of this 2D distribution possess line widths smaller than 100 Hz, indicating that lines have been narrowed by a factor of 30-40 when compared to the 1D MAS. The centers of mass of each centerband along ν_1 and ν_2 allow one to calculate the isotropic chemical and quadrupolar shifts of the two sites (eqs 12); line shape simulations of the anisotropic powder patterns (Figure 11) can then yield the individual e^2qQ/h and η contributions to ν_0^Q, summarized in Table 2 and in good agreement with literature data.[31]

Figure 12 illustrates additional examples of the characterization power of MQMAS NMR, this time on polycrystalline samples of Na_2SO_3, $Na_5P_3O_{10}$, and Na_2HPO_4. As in the case of the tellurite, conventional MAS can reduce substantially the line widths observed in a static ^{23}Na NMR experiment due to the successful removal of the homonuclear dipolar broadenings and scaling of second-order quadrupolar effects. Only with the use of MQMAS, however, can all the inequivalent sites in the different salts be successfully resolved and characterized. A common denominator of these experiments is the unequal intensities observed for the peaks in the various 2D NMR distributions. This heterogeneity originates mainly in the differences with which sites possessing different quadrupole

(31) Tagg, S. L.; Hoffman, J. C.; Zwanziger, J. W. *Chem. Mater.* **1994**, *6*, 1884.

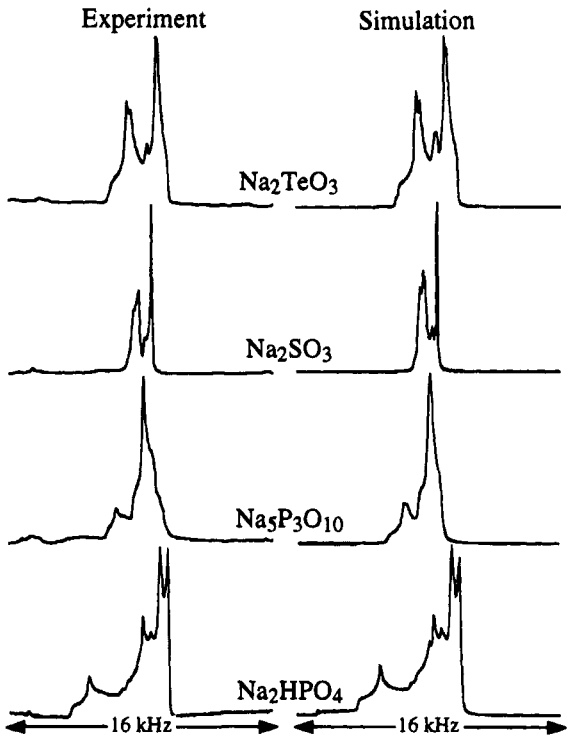

Figure 13. Quantitative fit of conventional MAS line shapes on the basis of MQMAS data. Simulations were obtained using the NMR parameters indicated in Table 2 and the following relative abundance ratios: Na_2TeO_3: site 1/site 2 = 1/1, Na_2SO_3: site 1/site 2/site 3 = 2/1/1, $Na_5P_3O_{10}$: site 1/site 2 = 1/3, Na_2HPO_4: site 1/site 2/site 3 = 1/1/2. Note that spectra in this figure are not referenced to $\delta_{NaCl} = 0$.

coupling constants are excited by the MQMAS pulse sequence, and makes it necessary to exercise special care when trying to discern the presence of peaks arising from sites with large quadrupolar coupling constants. This need is well exemplified by the spectrum of Na_2HPO_4, which we mistakenly analyzed in a previous publication[15] but whose peaks are now correctly identified in Figure 12. For the case of these sodium salts the fact that one of the spectral peaks is much stronger than the rest introduces minor artifacts in the anisotropic line shapes that can be extracted for the latter; the analysis of all the peaks is nevertheless straightforward (Table 2) and yields NMR parameters that are in good agreement with previous measurements on Na_2SO_3 and Na_2HPO_4.[32,33]

An important limitation of these MQMAS NMR spectra is their apparent lack of quantitativeness. Indeed the spectral results introduced in Figure 12 demonstrate that when a sample possesses sites with widely different quadrupole couplings, the strongly coupled sites can lead to much smaller spectral peaks than what could be predicted on the basis of their crystallographic abundance. This shortcoming can in principle be alleviated by means of two different strategies. One possibility is to increase the intensity of the nutation field ν_1 until the limit of similar excitation efficiencies for inequivalent sites is achieved; as evidenced in Figure 9, this can become an unrealistically challenging proposition for coupling constants in excess of 4 MHz. Alternatively, one could rely on the fact that the MQMAS experiment completely determines the parameters that define the conventional MAS line shape, in order to extract the relative intensities of the different sites from a best fit of the 1D MAS NMR spectrum. Such fitting procedure will be much less ambiguous than fitting an MAS line shape without any *a priori* information, since once the MQMAS data are analyzed only a small number of intensity parameters will remain to be found. Moreover, the 1D MAS line shape on which such quantitative fitting has to be performed can usually be acquired in a very reasonable amount of time using small excitation pulses,[34] thus freeing the analysis from nutation distortions. Figure 13 illustrates the results afforded by this fitting procedure when applied to the different sodium compounds that we analyzed here by MQMAS.

Conclusions

The preceding paragraphs presented a detailed discussion on the uses of 2D MQMAS toward the acquisition of high-resolution quadrupolar NMR spectra. Among the main conclusions of these investigations, it is worth remarking the experimental simplicity with which MQMAS can be used to resolve inequivalent sites, the possibility of using these data for discriminating isotropic chemical from isotropic quadrupolar shifts by simple inspection of the spectra, the reliable use of the anisotropic MQMAS spectral line shapes for extracting the quadrupolar parameters e^2qQ/h and η, the S/N advantages derived from employing optimized pulse lengths and the highest available levels of rf irradiation, and the possibility of carrying out quantitative analyses by combining the MAS and the MQMAS data. It can be expected that further improvements to the data processing and pulse sequence conditions described in this work will appear in the future, as the users of this simple methodology multiply.

Acknowledgment. We are grateful to Prof. J. P. Amoureux (Univ. Sci. and Tech. - Lille) and to Prof. P. J. Grandinetti (Ohio State Univ.) for valuable discussions regarding the acquisition and processing of MQMAS data. We also thank Dr. S. Hyberts (Molecular Simulations) for his assistance with the setup of NMRPipe. The present work was supported by the UIC Campus Research Board and by the National Science Foundation through grants DMR-9420458 and CHE-9502644 (CAREER Award). L.F. is a Camille and Henry Dreyfus New Faculty Awardee (1992−1997).

JA952925Y

(32) Power, W. P. *Magn. Reson. Chem.* **1994**, *33*, 220.

(33) Baldus, M.; Meier, B. H.; Ernst, R. R.; Kentgens, A. P. M.; Altenschildesche, H. M. z.; Nesper, R. *J. Am. Chem. Soc.* **1995**, *117*, 5141.

(34) Eenzke, D.; Freude, F.; Frohlich, T.; Haase, J. *Chem. Phys. Lett.* **1984**, *111*, 171.